Study of the thermal diffusivity of nanofluids containing SiO$_2$ decorated with Au nanoparticles by thermal lens spectroscopy

Ángel Netzahual-Lopantzi[1] · José Francisco Sánchez-Ramírez[2] · José Luis Jiménez-Pérez[1] · Delfino Cornejo-Monroy[3] · Genaro López-Gamboa[4] · Zormy Nacary Correa-Pacheco[5]

Abstract

In this work, silicon dioxide (SiO$_2$) spheres and gold nanoparticles (Au) were prepared. The SiO$_2$ was used as a platform to deposit the gold nanoparticles. The SiO$_2$ structures were synthesized employing the Stöber method. Monodisperse spherical particles with mean size of 293 nm were observed by transmission electron microscopy (TEM). The gold nanoparticles were attached to the dielectric platform trough in situ reduction. The UV–Vis spectrum of SiO$_2$–Au showed an absorption band in the visible region associated with the presence of the gold nanoparticles. The TEM micrographs confirmed decorated SiO$_2$ spheres with the metallic nanoparticles of 5 nm in size. Nanofluid concentrations of 0.1–0.6 mg/ml of SiO$_2$ decorated with Au nanoparticles dispersed in water were prepared. The functional groups of SiO$_2$-functionalized spheres were followed by FTIR. The formation of gold nanoparticles was evidenced by UV–Vis spectroscopy. The crystalline structure of SiO$_2$ spheres and SiO$_2$ decorated with Au nanoparticles was determined by XRD. The thermal diffusivity as a function of concentration using the mode-mismatched thermal lens (TL) spectroscopy was studied. The results of TL spectroscopy showed an increase in the thermal diffusivity with an increase of SiO$_2$ decorated with Au nanoparticle concentration in the nanofluid.

Keywords Thermal diffusivity · SiO$_2$ decorated · Au · Nanoparticles · Thermal lens

✉ José Luis Jiménez-Pérez
  jimenezp@fis.cinvestav.mx

[1] Unidad Profesional Interdisciplinaria en Ingeniería y Tecnologías Avanzadas-Instituto Politécnico Nacional, Av. Instituto Politécnico Nacional No. 2580, Col. Barrio La Laguna Ticomán, Del. Gustavo A. Madero, C.P. 07340 Mexico, D.F., Mexico

[2] Instituto Politécnico Nacional-CIBA, Ex-Hacienda San Juan Molino Carretera Estatal Tecuexcomac-Tepetitla, Km 1.5, C.P. 90700 Tlaxcala, Mexico

[3] Instituto de Ingeniería y Tecnología-Universidad Autónoma de Ciudad Juárez, Av. del Charro No. 450, C.P. 32310 Ciudad Juárez, Chihuahua, Mexico

[4] Universidad Politécnica del Valle de Toluca, Km 5.6 Carretera Toluca-Almoloya de Juárez, Santiaguito Tlalcilalcali, C.P. 50904 Almoloya de Juárez, Mexico

[5] CONACYT-Instituto Politécnico Nacional. Centro de Desarrollo de Productos Bióticos, Carretera Yautepec-Jojutla, km. 6, Calle CEPROBI, No. 8, San Isidro, Yautepec, C.P. 62731 Morelos, Mexico

1 Introduction

The silicon dioxide is one of the most abundant materials in nature, produced by plants and synthetically. It is widely used in the industrial area, as additive for hydrophobic textiles [1], anticorrosive coating [2] and as flame retardant [3]. In addition, it has also been implemented in the biomedical area due to its compatibility and low toxicity [4]. Nowadays, monodisperse SiO$_2$ particles can be synthesized quickly and efficiently using the Stöber method. This method involves the hydrolysis and condensation of tetraethyl orthosilicate (TEOS) under alkaline conditions in the presence of alcohol [5]. The physico-chemical properties of SiO$_2$ nanoparticles such as size and particle shape, photoluminescence, absorption coefficient, and silanol concentration determine some of their applications [6] for example, in the synthesis of nanofluids.

The nanofluids are liquid suspensions containing dielectric, semiconductors or metallic nanoparticles. In 2010, Tavman and co-workers [7] studied nanofluids containing nanoparticles of SiO$_2$ (at concentrations of 0.45 and 1.85 vol.%) with average size of 12 nm dispersed in deionized water.

They found that the effective thermal conductivity was improved with respect to the base fluid. In recent years, the thermal diffusivity of SiO_2 nanofluids has been investigated. Some authors reported that for a volume concentration of 1–3% of SiO_2, a thermal diffusivity value of 15×10^{-4} cm^2/s was found. They suggest that convection was the main mode of heat transfer [8]. On the other hand, gold nanofluids had a thermal diffusivity value of 26×10^{-4} cm^2/s with particle average size of 30 nm [9] that was higher than for the nanofluids mentioned above. In 2016, Jhon and co-workers [10], prepared nanofluids containing aggregates of Au-ssDNA (single-stranded DNA) of 20 nm obtained via green synthesis, that were measured by dual beam thermal lens technique. The thermal diffusivity values revealed an increase in the values for higher molar concentration of ssDNA. The main disadvantage was that the DNA was more expensive than SiO_2. However, the thermal resistance of SiO_2 nanofluid was subsequently reduced by immersion in a liquid media of SiO_2–Au nanoparticles.

Nanostructures formed from a dielectric material and gold nanoparticles are a new class of plasmonic materials that are attracting interest in new research, because metal structures deposited on a substrate are more stable and aggregation decreases without affecting the results obtained. In 2002, Gu and co-workers [11] prepare decorated SiO_2 macroporous films with gold nanoparticles (10 nm). Films were deposited on glass substrate with SiO_2 spheres of average size of 195 or 300 nm. Then, the glass containing SiO_2 was immersed in a gold solution to decorate the macroporous films. The UV–Vis spectra of the decorated films showed an intense absorption band in the visible region around 527 nm confirming the immobilization of metal nanostructures on SiO_2 films. On the other hand, in 2013, Convertino et al. [12] obtained decorated SiO_2 nanowires with Au nanoparticles (30–50 nm) and Ag nanoparticles (80–130 nm) by evaporation of thin metallic films on wires. The dielectric showed high reflectivity values of 45–55% in the visible region, decreasing the reflectance to 10% after the decoration process with metal nanoparticles. The decrease of reflection occurred at wavelengths of 525 nm and 370 nm for gold and silver, respectively, in agreement with the selective absorption of surface plasmon resonance (SRP). Therefore, the authors suggest multiple light scattering events, i.e., the decorated nanowire multiply the light path several times in a random path inside the decorated structure, phenomenon that was called light trapping.

Other routes have also been employed for the synthesis of decorated SiO_2 structures. The chemical route has been used with the help of silanol groups because they have the ability to form covalent bond with species like 3-aminopropyl-triethoxysilane (APTES) or 3aminopropyltrimethoxysilane (APTMS), leaving an amino group (–NH_2) in the surface and attracting other chemical species [1, 13]. The new plasmonic

materials as base for SiO_2–Au reported in the last years serve as carriers for DNA in non-viral administration-targeted systems, reporting higher cell transfection values compared to commercial reagents and excluding cytotoxicity [14]. In addition, it offers advances in biosensors, immobilizing antibodies of bovine serum albumin (Anti-BSA) detected by changes in the refractive index [12]. Finally, this SiO_2–Au structure showed an enhancement of light absorption around to the frequency of SRP of metallic nanoparticles [15].

In this work, the decoration of SiO_2 spheres with gold nanoparticles was achieved and the thermal diffusivity was determined for nanofluids containing different concentrations of SiO_2–Au, using the thermal lens spectroscopy technique. Then, new nanofluids with better thermal properties than conventional nanofluids were obtained.

2 Experimental setup and methodology

The reagents used for the preparation of the SiO_2–Au spheres were: tetraethyl orthosilicate (TEOS, 99%), ammonium hydroxide (NH_4OH, 28–30% as ammonia NH_3) (3-aminopropyl) triethoxysilane (APTES), tetrachloroauric acid ($HAuCl_4 \cdot 3H_2O$, 99.99%), sodium borohydride ($NaBH_4$ 98%) and sodium citrate dehydrate (OHC (COONa) (CH_2 COONa)$_2$ 2H$_2$O, 99%). All were purchased from Sigma Aldrich. Methanol (CH_3OH 99%), ethanol (C_2H_5OH 99%), and sodium hydroxide (NaOH 99%) were obtained from J.T. Baker. Deionized water was employed for preparing the solutions (Millipore system, with water resistivity of 18.2 MΩ cm).

2.1 Synthesis of SiO_2 spheres

The monodisperse SiO_2 spherical structures were prepared using the Stöber method 1968 [5]. The method involves the hydrolysis and condensation of TEOS under alkaline conditions in the presence of ammonia (NH_3) as a catalyst agent.

The SiO_2 nanoparticles were synthetized employing the TEOS as molecular precursor of silicon. 60 ml of a solution containing ethanol (14.4 mol/l), TEOS (0.037 mol/l), water (5.9 mol/l), and ammonia (1.6 mol/l) were prepared. The reactant solution was subjected to vigorous agitation (300 rpm) for 12 h at room temperature to carry out the process of hydrolysis and condensation of TEOS. The resulting colloidal suspension was centrifuged (12,000 rpm, for 15 min). The particles in methanol/water at a volumetric ratio 1/1 were recovered, repeating the process at least 5 times. Finally, the SiO_2 nanoparticles were dispersed in ethanol to obtain a colloidal solution with a weight ratio of 20:80, respectively.

2.2 Functionalization

The surface functionalization of the SiO_2 nanospheres was carried out by grafting the –OH groups with the –NH_2 amino groups [12]. Then, 0.012 mol/l of APTES was prepared in ethanol/water, and mixed with the SiO_2 spheres solution with volume ratio 7/3 under vigorous stirring at a constant temperature of 80 °C for 1 h. The obtained mixture was cooled to room temperature and subjected to a centrifugation process (8000 rpm for 30 min) and rinsed (with a water/ethanol solution = 1/1 v/v) to eliminate excess APTES. The wash was repeated five times. Finally, 0.3 g of functionalized SiO_2 spheres was mixed in water (1 ml) and stored at room temperature for further use.

2.3 Preparation of SiO₂ decorated with gold

The decoration of SiO_2 spheres with Au nanoparticles was carried out in two steps: first a gold precursor solution was prepared. It was obtained mixing sodium hydroxide (0.1 mol/l) with a solution of $HAuCl_4$ (6.35 mol/l) for 15 min under stirring. A pH 8 was used to hydrolyze the Au–Cl bonds with the successive formation of gold hydroxide $Au(OH)^-_3$. As a second step, 0.25 ml of the solution of amino-functionalized SiO_2 spheres was added to 10 ml of the gold hydroxide solution. The mixture was then heated at 70 °C for 30 min under stirring to accelerate the homogeneous deposition of gold hydroxide $Au(OH)^-_3$ on the surface of SiO_2 spheres [13]. 0.015 g of SiO_2 decorated with $Au(OH)_3$ was dissolved in 20 ml of water inside a flask. Then, 10.5 ml of $NaBH_4$ was added (6.6 mol/l) and 5.25 ml of dehydrate sodium citrate (10 mol/l) to reduce $Au(OH)_3$ in $Au°$ over SiO_2. The obtained SiO_2 decorated with gold nanoparticle samples were centrifuged at 8000 rpm for 1 h and rinsed with deionized water five times. Then, the samples were dried until a powder was obtained. Different concentrations in weight = 0.1, 0.2, 0.3, 0.4, 0.5 and 0.6 mg of SiO_2–Au in 1 ml of deionized water were used to prepare the nanofluids.

2.4 Characterization

For the characterization of the optical and structural properties of SiO_2 and SiO_2–Au, different techniques were used: UV–Vis spectroscopy (spectrophotometer Genesys 10S, Thermo Scientific), Fourier transform infrared spectroscopy (FTIR) (Vertex 70, Bruker) through the attenuated total reflectance technique (ATR), X-ray diffraction (XRD) (Rigaku, Smartlab) and transmission electron microscopy (TEM, model JEOL JEM 1010). The optical measurements were made on samples dispersed in water. For FTIR and X-ray measurements, powder samples were characterized in a range of 400–4000 cm^{-1} and angular range of 10–80° with a step size of 0.02° for 2θ, respectively. For TEM, each of the colloidal samples was deposited on a copper grid (covered with a FORMVAR film) until the solvent was evaporated at room temperature.

2.5 Characterization by thermal lens

The thermal diffusivity was determined by thermal lens (TL). This technique involves the incidence of an excitation laser beam with a Gaussian profile that induces a temperature distribution in the sample. The heat generated in the center of the sample is caused by the intensity of the laser at this point, so a temperature gradient and a change in the refractive index occur. This behaves like a convergent or divergent lens when a second or probe laser beam, of less intensity, passes through that point. This produced an effect called thermal lens [16, 17].

The experimental set up of thermal lens is shown in Fig. 1. The measurement of the TL signal was carried out using an Ar^+Xe laser (514 nm and 40 mW) as an excitation laser and a second laser of He–Ne (632 nm and 0.9 mW) as a probe laser. A mechanical shutter was used to limit the excitation light beam to the sample. This was focalized by a lens of 25-cm focal length in a liquid sample contained in a 1-cm long quartz cuvette, positioned in the focal plane. A second aligned probe laser, and deflected at a small angle, was focused by a 10 cm lens, oppositely directed to the excitation laser.

The light from the transmitted probe beam was recorded by a photodiode (PD). The sensor was coupled to a National Instrument card to record the time evolution of the thermal lens signal. Labview software was used to control and capture TL data and normalize this signal with respect to the initial time signal. The experimental data were adjusted
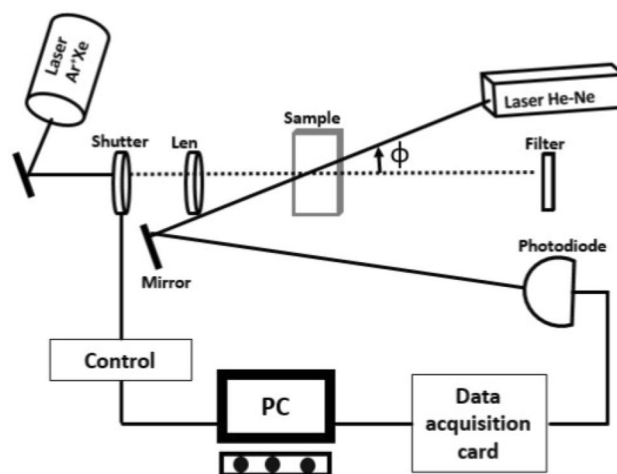

Fig. 1 Experimental setup for mode-mismatched dual-beam thermal lens spectroscopy

using the theoretical Eq. (1) with θ and the constant t_c (characteristic time of TL) as adjustment parameters. Hence, the thermal diffusivity of the sample was calculated from Eq. (1). This process was used for all the experimental data to obtain the thermal diffusivity of the samples.

2.5.1 Theory

The intensity of the probe beam transmitted from the center of the sample in the presence of the excitation laser was derived from a theoretical expression that was developed by Shen et al. [18] using a relation for the signal $I(t)$ with a diffraction approximation for the Gaussian beam in the following way:

$$I(z,t) = I_0\left(1 - \theta \tan^{-1}\left(\frac{2mV}{[(1+2m)^2 + V^2]\frac{t_c}{2t} + 1 + 2m + V^2}\right)\right)^2,$$
(1)

where

$$V = \frac{Z_1}{Z_c}, \quad m = \left(\frac{w_p}{w_e}\right)^2, \quad t_c = \frac{w_e^2}{4D}, \quad \theta = \frac{P_e\,\alpha l}{k\lambda_p}\frac{d_n}{d_T},$$
(2)

where $I(t)$ is the signal transmitted from the probe beam to the detector as a function of time and normalized with $I(0)$ which is the initial intensity of $I(t)$, $Z_1 =$ *is the distance from the probe beam waist to the sample*, $Z_c = w_p^2/\lambda_p$ is the confocal distance (cm), w_p $(1.81 \times 10^{-2}$ cm) and w_e $(4.8 \times 10^{-3}$ cm) are the ratio of the probe and excitation beam of the sample, respectively, t_c is the characteristic thermal time constant, λ_e and λ_p are the wavelength of the excitation and probe beam, respectively, D and k are the diffusivity and the thermal conductivity of the sample, P_e is the power of the excitation beam, α is the absorption coefficient and l is the thickness of the sample (1 cm). dn/dT is the refractive index dependent on the temperature of the sample. For the thermal measurements, the nanofluids were subjected to ultrasonication to ensure a correct dispersion of the nanoparticles.

3 Results and discussion

3.1 TEM for SiO$_2$ nanoparticles

Figure 2 shows the TEM micrographs of SiO$_2$ particles obtained for 1.6 mol/l ammonium catalyst using the Stöber method (1968). Structures well defined with spherical shape were observed. The SiO$_2$ spheres with an average size of 293 nm are showed in the histogram (Fig. 2) for which 60 nanoparticles were counted. The monodispersity ($\sigma < 20\%$) of the SiO$_2$ nanoparticles is seen in the size distribution histogram from Fig. 2. The formation of SiO$_2$ spheres, average size and monodispersity are in agreement with those reported by the other authors [19, 20].

3.2 FTIR

The functional groups of SiO$_2$ functionalized with APTES were determined by FTIR spectroscopy. In Fig. 3, the spectra of SiO$_2$ particles showed absorption peaks corresponding to vibrational frequencies in the SiO$_2$. The peak at 550 cm^{-1} is related to longitudinal optical vibration of Si–O–Si, the vibrational mode corresponding to symmetric tension Si–O–Si is observed at 800 cm^{-1}, the bands at 1080 cm^{-1} and at 1200 cm^{-1} are attributed to asymmetric tension in and out of phase for Si–O–Si, respectively [21, 22]. The vibrational frequency located at 955 cm^{-1} is related to bond tension Si–OH and its intensity show the amount –OH groups on surface of the nanosphere [23]. Finally, the absorption bands corresponding to vibrational frequency of bending and stretching of water bond on surface of spheres SiO$_2$ are located at 1640 cm^{-1} and 3362 cm^{-1} [24].

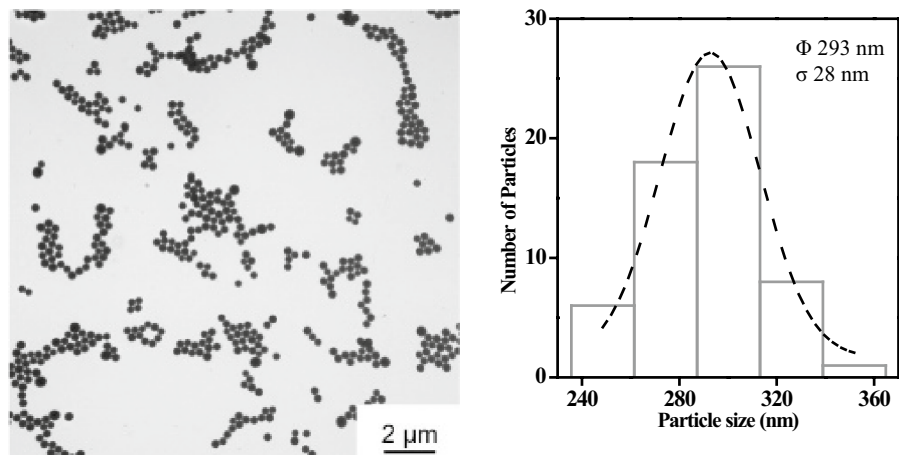**Fig. 2** TEM micrograph and size distribution histogram of SiO$_2$ particles

Fig. 3 FTIR spectra to **a** SiO$_2$ functionalized with APTES and **b** only APTES
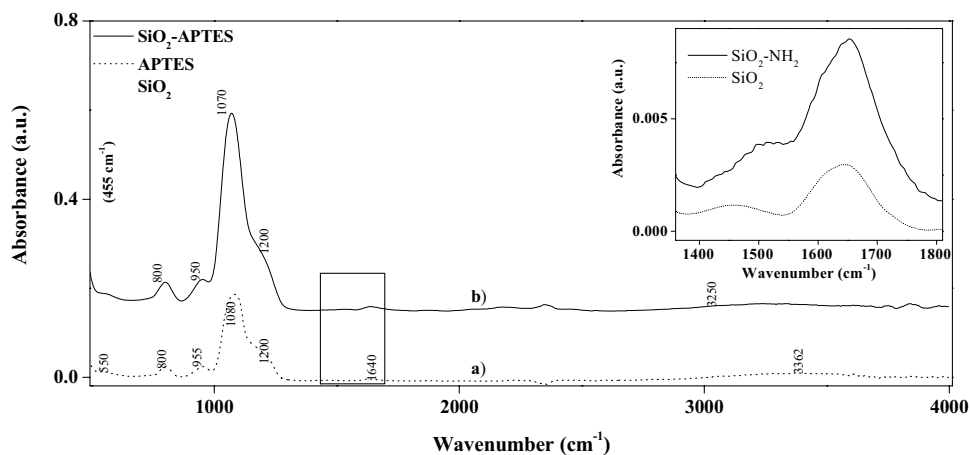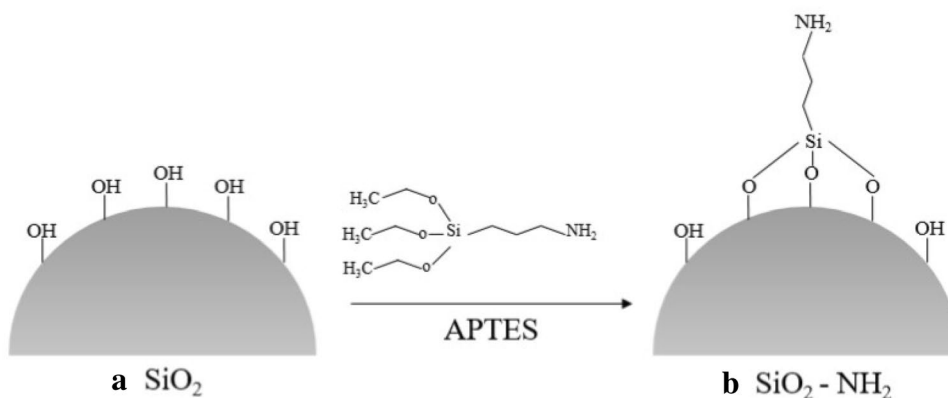

Fig. 4 Schematic representation of SiO$_2$ spheres; **a** before and **b** after functionalization with amino groups

A schematic representation of SiO$_2$ sphere functionalized surface is observed in Fig. 4. It shows the spheres surface as obtained after synthesis process using the Stöber method (a), and for a post-synthesis surface modification by adding APTES (b). In this work, FTIR spectra of the spheres without and with amine grafted on surface were compared, finding in the latter a peak around 1510 cm^{-1} attributed to the presence of the amine group (–NH$_3^+$) [25], which is observed in the insert in Fig. 3.

3.3 UV–Vis spectroscopy

Amine group were grafted over SiO$_2$ spheres. When these amine are protonated, they acquire positive charge –NH$_3^+$ and it is well know that they have affinity for negative charges such as gold hydroxide (Au(OH)$^-_3$) [13, 26] for pH 8. Once this condition is fulfilled, the gold complexed fall over functionalized SiO$_2$ spheres, i.e. SiO$_2$ decorated with Au(OH)$_3$ molecules, in the presence of sodium borohydride, gold hydroxide was reduced to Au°. In this work, the products obtained in each step were monitored by UV–Vis spectroscopy. The UV–Vis spectra of SiO$_2$ spheres after synthesis using the Stöber method (a) is shown in Fig. 5. The
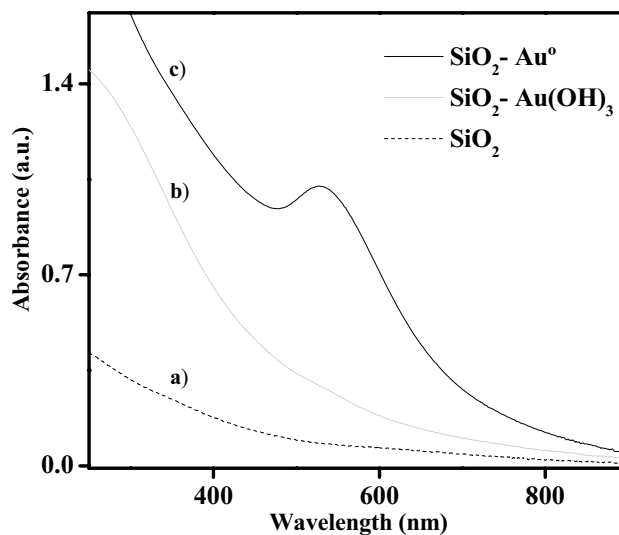

Fig. 5 UV–Vis spectra for **a** SiO$_2$ spheres, **b** SiO$_2$–Au (OH)$_3$ complex, **c** Au° nanoparticles deposited on SiO$_2$

absence of an absorption peak in visible region is observed [6]. The same behavior was obtained for SiO$_2$–Au(OH)$_3$.

When the $Au(OH)_3$ was reduced, a color change from orange–brown to red was observed, as indicative of gold nanoparticle formation. Therefore, by UV–Vis spectroscopy a band around to 517 nm was registered confirming the formation of gold nanoparticles. This band is associated with surface plasmon resonance (SRP).

3.4 TEM for SiO$_2$–Au nanoparticles

The SiO$_2$–Au nanoparticles were investigated by TEM microscopy. In Fig. 6, gold nanoparticles deposited on surface of SiO$_2$ spheres with spherical shape are clearly observed. According to the histogram of Fig. 6, the gold nanoparticle mean size was 4.8 nm, with similar values to those reported by Kah et al. 2008 [13]. Moreover, the standard deviation of gold nanoparticles revealed a high monodispersity in size distribution. Thus, UV–Vis spectra and TEM micrograph showed gold nanoparticle immobilization over SiO$_2$ spheres, by using a quickly and an efficiently chemical

synthesis for the in situ process of SiO$_2$. For the histogram, 30 particles of each SiO$_2$ sphere were counted and the average diameter of the gold particles was estimated, as can be seen in Fig. 6.

3.5 XRD

X-ray diffraction spectra were obtained for SiO$_2$ spheres with and without decorate. The CCDC/FIZ Karlsruhe assigned deposition service number was CCDC 1881812. In Fig. 7, SiO$_2$–Au structures present four peaks of metallic gold located at 37.8 (111), 45.9 (200), 67.2 (220), and 76.5° (311) [9], for the face cubic-centered structure of gold nanoparticles over SiO$_2$. The crystalline structure of the sample is well defined by the sharp peaks, in particular, those related to metallic Au (JCPDS, No. 9011612) [27]. On the other hand, the inset in Fig. 7 shows the spectrum for the dielectric material with an amorphous structure.

Fig. 6 TEM micrograph and size distribution histogram of gold nanoparticles deposited on SiO$_2$ spheres
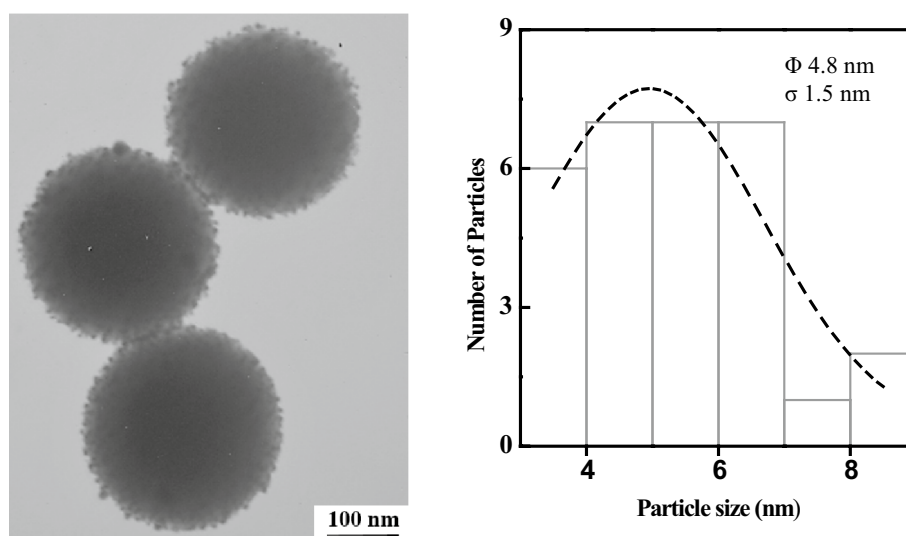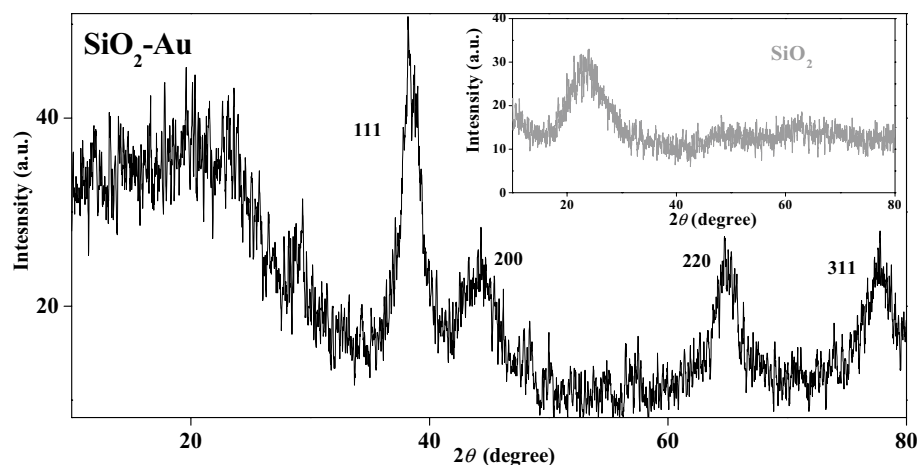

Fig. 7 XRD pattern of the SiO$_2$ spheres decorated with gold nanoparticles and insert for SiO$_2$ spheres

3.6 Thermal lens (TL)

The colloidal structures synthesized were centrifuged and dried to obtain powders. Nanofluids were elaborated containing SiO$_2$–Au in deionized water, for different concentrations ranging from 0.1 to 0.6 mg/ml. In Fig. 8, a typical spectra of thermal lens evolution vs time of nanofluids containing SiO$_2$–Au dispersed in water are shown. The system was calibrated with water. The theoretical curve of the spectra was calculated with Eq. (1) and the experimental data were fitted to Eq. (1), with characteristic time (t_c) of TL in milliseconds, similar to reported by Lenart et al. 2018 [28].

The parameters θ and t_c were obtained fitting the normalized thermal lens signal as function of time and the thermal diffusivity was calculated employing the Eq. (2). Thermal diffusivity values were between $15.59 \pm 0.23 \times 10^{-4}$ cm^2/s to $28.60 \pm 0.61 \times 10^{-4}$ cm^2/s. The values for the characteristic time (t_c) range from $3.85 \pm 0.05 \times 10^{-3}$ s to $2.10 \pm 0.04 \times 10^{-3}$ s and for θ, from $5.82 \pm 0.20 \times 10^{-2}$ to $2.88 \pm 0.34 \times 10^{-2}$ for SiO$_2$–Au concentrations of 0.1 to 0.6 mg/ml, as shown in Table 1. All the nanofluids values obtained were higher than the thermal diffusivity of the water-base fluid, which was deionized water (14.2×10^{-4} cm^2/s) [29]. In Fig. 9, it can be seen that the thermal diffusivity of the nanofluid increased with concentration of nanostructures (SiO$_2$–Au). Also, the thermal diffusivity for SiO$_2$ nanofluids of 300 nm at a concentration of 0.37 mg/ml, measured in a previous work is shown in Fig. 9 with

Table 1 Parameters obtained by thermal lens spectroscopy of SiO$_2$–Au nanofluids

Sample in Fig. 8	Concentration (mg/ml)	D ($\times 10^{-4}$ cm^2/s)	t_c ($\times 10^{-3}$ s)	θ ($\times 10^{-2}$)
a	0.1	15.59 ± 0.23	3.85 ± 0.05	5.82 ± 0.20
b	0.2	19.51 ± 1.19	3.08 ± 0.16	9.08 ± 0.50
c	0.3	22.95 ± 0.33	2.61 ± 0.03	8.30 ± 0.30
d	0.4	25.94 ± 0.38	2.31 ± 0.03	4.90 ± 0.16
e	0.5	27.10 ± 0.42	2.21 ± 0.03	4.06 ± 0.14
f	0.6	28.60 ± 0.61	2.10 ± 0.04	2.88 ± 0.34

a star symbol. The obtained value was 17.51×10^{-4} cm^2/s [16]. The best fitting for the experimental values was a linear function, $D = 1.42 \times 10^{-3}$ (cm^2/s) $+ 2.59 \times 10^{-3}$ (cm^2/s) C (mg/ml) ($D =$ thermal diffusivity; $C =$ SiO$_2$–Au concentration). However, it is necessary to propose new models to explain this thermal behavior for the studied system.

The behavior of the thermal diffusivity as a function of SiO$_2$–Au nanoparticle concentration (Fig. 10) can be explained as follows. The first reason is that the light within SiO$_2$ spheres (Fig. 10a) and SiO$_2$ structures decorated with Au nanoparticles (Fig. 10b) follows a different path. Inside SiO$_2$–Au particles, the light is trapped because it follows a random path many times. This is because each gold nanoparticle folds the light and the process is presented more often than for SiO$_2$ spheres. This phenomenon increases the
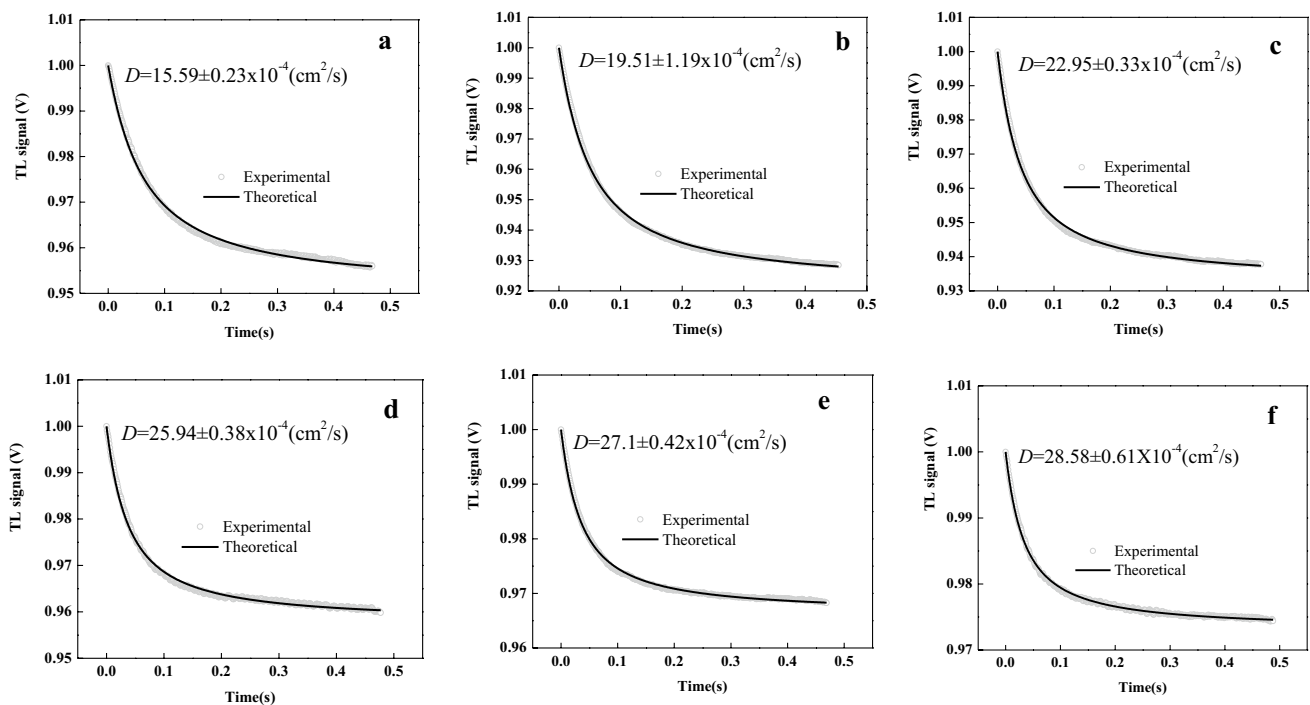

Fig. 8 Thermal lens signal for SiO$_2$–Au nanofluids concentrations: **a** 0.1, **b** 0.2, **c** 0.3, **d** 0.4, **e** 0.5 and **f** 0.6 mg/ml
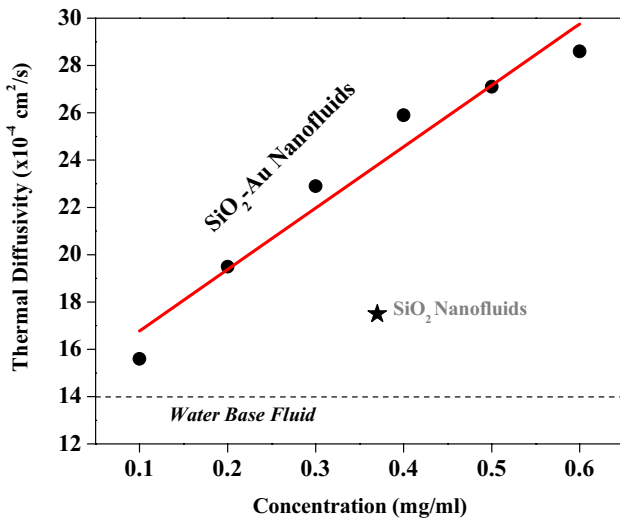
Fig. 9 Thermal diffusivity of SiO$_2$–Au nanofluids as a function of concentration

absorption of the light in the visible region confirmed by the spectra of Fig. 5. Convertino et al. 2013 [12] observed a similar effect. They reported optical reflectance modification of SiO$_2$ nanowires decorated with gold and silver nanoparticles, registering a decreased reflectivity of the SiO$_2$–Au nanowires, compared with nanowires without decorate, attributing

to optical phenomenon called light trapping. In other words, there is an increase of light absorption due the presence gold nanoparticles on nanowires when reflectivity decreases. They derived a model explaining the spectral range where the nanoparticle/nanowire structure is absorbing as function of the reflectivity R. R is inversely proportional to the wire absorption coefficient, α, with $R \approx \frac{1}{N\alpha d}$, where N is the number of particles and d is the diameter of nanoparticles. The second reason is the thermal response of the material to a change in temperature measured by the thermal diffusivity (D), which can be defined as $D = k/\rho c_p$. In the equation, k is the thermal conductivity, ρ is the mass density and c_p is the specific heat capacity. The thermal diffusivity is an important property related to the rate of heat transfer followed by the absorption of electromagnetic radiation [30]. The thermal conductivity of the nanofluids depends on factors such as the size and the concentration of the nanoparticles due to the high surface-to-volume ratio of nanoparticles [29, 30]. The thermal conductivity increases due to the gold nanoparticles, which covers the SiO$_2$ spheres. Then, the increase in thermal diffusivity is favored for a higher concentration of SiO$_2$–Au. This thermal enhancement also could be related to phonon scattering phenomenon across the liquid–solid interface. The excited electrons lose excess energy in the form of phonons (collective oscillations of elastic waves that propagate through the material). As a consequence, the
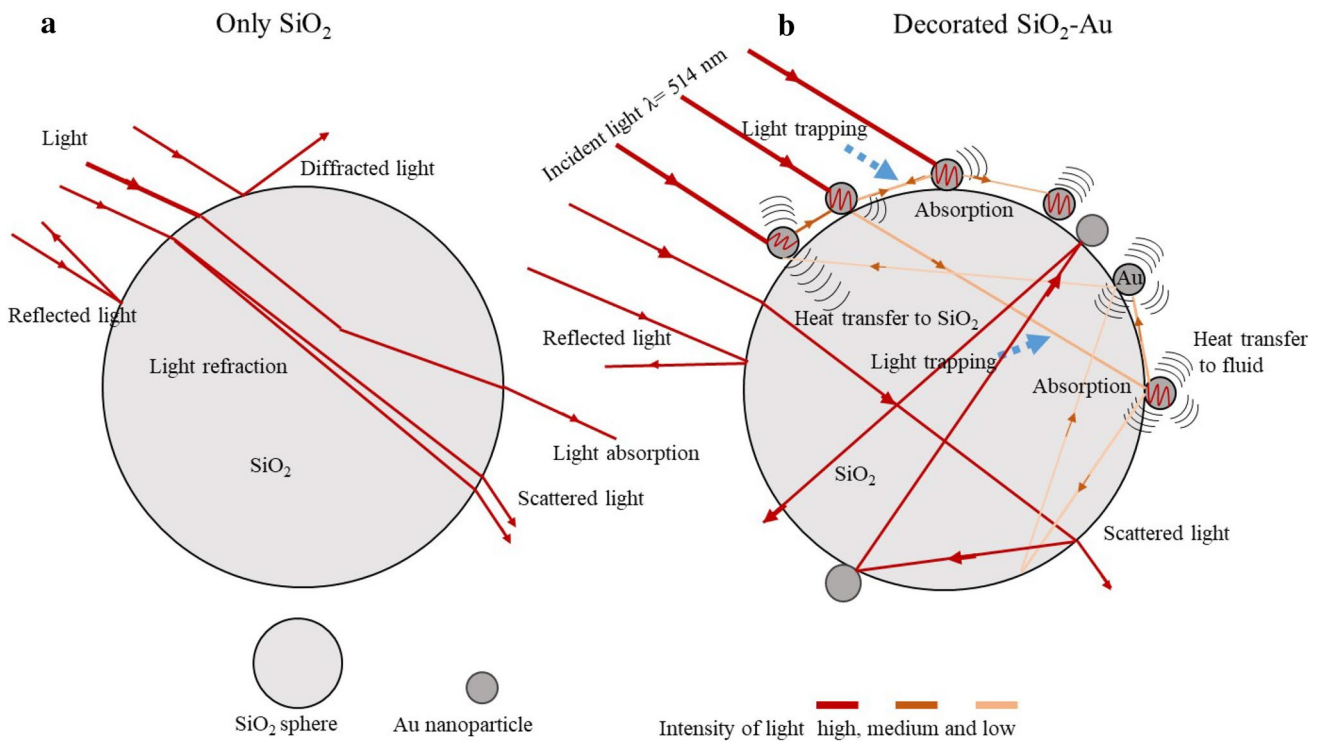

Fig. 10 Schematic representation of the possible path light within of **a** SiO$_2$ spheres and **b** light trapping for SiO$_2$ structures decorated with Au nanoparticles

heat is dissipated from the nanoparticles to the surrounding medium. Therefore, at higher nanoparticle concentration per volume unit, the higher amount of energy is generated and transferred to the nanofluid [31–33].

4 Conclusions

Gold nanoparticles attached to the surface of a SiO$_2$ dielectric platform were synthesized. This was achieved by changing the surface chemical composition of SiO$_2$ by grafting the terminal –OH by amino group –NH which attracts gold complexes, generating SiO$_2$–Au structures. Their synthesis was confirmed by UV–Vis spectroscopy, FTIR, TEM microscopy and XRD. The new class plasmonic structures were used to elaborate nanofluids containing 0.1–0.6 mg/ml in water, and the thermal diffusivity was measured by thermal lens spectroscopy. The results showed an increase of thermal diffusivity with SiO$_2$–Au concentration. The SiO$_2$–Au nanofluids had a higher value in thermal diffusivity than nanofluids containing only SiO$_2$ spheres with equivalent sizes for similar concentrations. That suggests that by immobilizing gold nanoparticles on SiO$_2$ spheres, the light that passes through of SiO$_2$–Au structures follows a multiple path due to the presence of gold nanoparticles on dielectric, causing a major light absorption and increasing heat transfer to the surrounding fluid, in this case, water. Therefore, is necessary to propose new models to explain this thermal behavior. Finally, this type of nanostructure synthesized could be employed in biosensors, because the optical absorption tuned in the visible region. This investigation also has applications in the treatment of cancer cells treated by photothermal effects.

References

1. C. Xue, S. Jia, J. Zhang, L. Tian, Thin Solid Films **517**, 4593 (2009)
2. S. Ammar, K. Ramesh, B. Vengadaesvaran, S. Ramesh, A. Arof, Electrochim. Acta **220**, 417 (2016)
3. Z. Fanglong, X. Qun, F. Qianqian, L. Rangtong, L. Kejing, Surf. Coat. Tech. **294**, 90 (2016)
4. I. Kim, E. Joachim, H. Choi, K. Kim, Nanomed-Nanotechnol. **11**, 1407 (2015)
5. W. Stöber, A. Fink, J. Colloid Interf. Sci. **26**, 62 (1968)
6. I. Rahman, P. Vejayakumaran, C. Sipaut, J. Ismail, C. Chee, Mat. Chem. Phys. **114**, 328 (2009)
7. I. Tavman, A. Turgui, M. Chirtoc, K. Hadjov, O. Fudym, S. Tavman, Heat Transfer Res. **41**(3), 209 (2010)
8. A. Abdelrazek, O. Alawi, S. Kazi, N. Yusoff, Z. Chowdhury, A. Sarhan, Int. Commun. Heat Mass Transfer **95**, 161 (2018)
9. E. Shahriarr, A. Bahrami, M. Varnamkaste, K. Behzad, SYLWAN **158**(6), 333 (2015)
10. J. Jhon, L. Thomas, A. Kurian, A. George, R. Soc. Chem. **6**, 62390–62398 (2016)
11. Z. Gu, R. Horie, S. Kubo, Y. Yamada, A. Fujishima, O. Sato, Angew Chem. Int. **41**, 1153 (2002)
12. A. Convertino, M. Cuscunà, F. Martelli, M. Manera, R. Rella, ACS **118**, 685 (2014)
13. J. Kah, R. Wang, J. Song, T. White, S. Mhaisalkar, I. Ahmad, C. Sheppard, M. Olivo, Gold Bull. **41**(1), 23 (2008)
14. L. Wang, T. Cheang, S. Wang, Z. Hu, Z. Xing, W. Qu, A. Xu, J. Mater. Res. **27**(18), 2425 (2012)
15. A. Colombelli, M. Manera, A. Taurino, M. Catalano, A. Convertino, R. Rella, Sensors Actuat. B-Chem. **226**, 589 (2016)
16. J.L. Jiménez-Pérez, J.F. Sánchez-Ramírez, D. Cornejo-Monroy, R. Guitierrez-Fuentes, J.A. Pescador-Rojas, A. Cruz-Orea, C. Jacinto, Int. J. Thermophys. **33**, 69 (2012)
17. R. Carbajal-Valdez, J.L. Jiménez-Pérez, A. Cruz-Orea, Z.N. Correa-Pacheco, M. Alvarado-Noguez, I.C. Romero-Ibarra, J.G. Mendoza-Alvarez, Thermochim. Acta **657**, 66 (2017)
18. J. Shen, R. Lowe, R. SnookR, Chem. Phys. **165**, 385 (1992)
19. T. Matsoukas, E. Gulari, J. Colloid Interf. Sci. **124**(1), 252 (1988)
20. D. Cornejo-Monroy, J.A. Pescador-Rojas, J.F. Sánchez-Ramírez, J.L. Herrera-Pérez, Rev. Sup. Vac. **22**(3), 44 (2009)
21. A. Bertoluza, C. Fangano, M. Morelli, J. Non-Cryst, Solids **48**, 117 (1982)
22. M. Gunde, Phys. B **292**, 286 (2000)
23. J.L. Montaño-Priede, J.P. Coelho, A. Guerrero-Martínez, O. Peña-Rogriguez, U. Pal, J. Phys. Chem-US **121**, 9543 (2017)
24. S. Wang, D. Wang, S. Smart, J. Diniz da Costa, Sci. Rep-UK **5**, 1 (2015)
25. S. Shou-Cang, K. Wai, L. Chia, D. Yuan-Cai, B. Tan, Mat. Res. Bull. **46**, 1665 (2011)
26. C. Chang, Y. Cheng, Y. Chuin-Tih, Appl. Catal. A-GEN **174**, 13 (1998)
27. A. Lanje, S. Sharma, R. Pode, J. Chem. Pharm. Res. **2**(3), 478 (2010)
28. V. Lenart, N. Astrath, R. Turchiello, G. Goya, S. Gómez, J. Appl. Phys. **123**(8), 1 (2018)
29. D.H. Kumar, H.E. Patel, V.R.R. Umar, T. Sundararajan, T. Pradeep, S. Das, Phys. Rev. Lett. **93**, 144301 (2004)
30. Z. Zheng, L. Qiu, G. Su, D. Tang, Y. Liao, C. Yunfa, J. Nanopart. Res. **13**(12), 6887 (2011)
31. E. Shahriari, M. Moradi, M. Raeisi, J. Theor. Appl. Phys. **10**(4), 259 (2016)
32. X. Huang, M. Alexandria, J. Med. **49**, 1 (2011)
33. N. Chandrasekharan, P. Kamat, J. Hu, G. Jones, J. Phys. Chem. B **104**, 11103 (2000)